P3.5 REMOTE SENSING OF MULTILAYER CIRRUS CLOUD PROPERTIES DURING INCA USING ATSR-2 DATA: CASE STUDY ON 23 MARCH 2000

Albano González[1], Peter Wendling[2], Bernhard Mayer[2]
Jean-Francois Gayet[3], Tom Rother[4]

[1]Dpto. Física FEES, Universidad de La Laguna, La Laguna, Spain
[2]Institut für Physik der Atmosphäre, DLR, Oberpaffenhofen, Germany
[3]Laboratoire de Météorologie Physique, Université Blaise Pascal, Clermont-Fd, France
[4]Institut für Methoden der Fernerkundung, DLR, Oberpfaffenhofen, Germany

1. INTRODUCTION

There are still large uncertainties on the optical and radiative properties of cirrus clouds which are an important component in the climate system of the earth/atmosphere. To improve our knowledge on this, cirrus cloud properties are needed on the global scale requiring the use of satellite data. However, most of the retrieval techniques developed up to now were limited to single layer cloud systems (Ou et al. 1993; Ou et al., 1999; Rolland et al., 2000). On the other hand in about half of all observations clouds occur in multilayer systems (Mace et al., 1997). Therefore, we present in the following a new retrieval based on the use of ATSR-2 data allowing to determine cirrus cloud optical thickness, effective ice particle size as well as the dominant ice crystal shape for the extreme case of an optically thin cirrus layer over a variable low water cloud. For this purpose we present a case study carried out near Punta Arenas within the frame of the EC funded project INCA (Interhemispheric Differences in Cirrus Properties from Anthropogenic Emissions). Within the study concomitant aircraft measurements are evaluated in combination with ATSR-2 data.

2. INSTRUMENTATION AND MEASUREMENT

2.1 *Aircraft Measurements*

During the INCA campaign measurements were carried out with four instruments mounted onboard the German research aircraft Falcon in order to determine microphysical and optical cirrus cloud properties: the PMS FSSP-300 optical particle counter (Baumgardner et al., 1992) for particles from 0.3 to 20 µm diameter, the PMS 2D-C probe (Knollenberg, 1981; Gayet et al., 1996) for the size range from 25 to 800 µm, and the polar nephelometer (Gayet et al., 1997; Auriol et al., 2001). In addition, the Falcon was equipped with standard meteorological and navigation instruments.

The selected flight on 23 March 2000 was located over the Pacific Ocean near the coast of Southern Chile. One part of the flight track was almost completely within cirrus clouds, and ascents and descents through the cirrus cloud layer were performed. The aircraft trajectory started at 15:07 UTC near 55°S, 71°W and finished at 15:25 UTC near 54°S and 74°W. The whole flight track was divided into three legs that correspond to different ambient conditions and altitudes. The three flight legs are presented in Figure 1 superimposed to the ATSR-2 image.

2.2 *ATSR-2 Data*

The Along Track Scanning Radiometer (ATSR-2) onboard the European Remote Sensing Satellite (ERS-2) has seven spectral bands centred at the wavelengths 0.55, 0.67, 0.87, 1.6, 3.7, 10.8 and 11.9 µm. It has been designed to observe the same scene in near nadir (zenith angle between 0 and 22°) and forward (52 – 55°) views using a conical scanning geometry (Prata et al., 1990). The forward image is measured approximately two minutes before the nadir image. The spatial resolution at the subsatellite point is about 1 km while the pixel size is about 3 – 4 km for the forward view. The data are supplied to users geolocated to a grid of 1 x 1 km^2 pixels, where forward and nadir images are coincident.

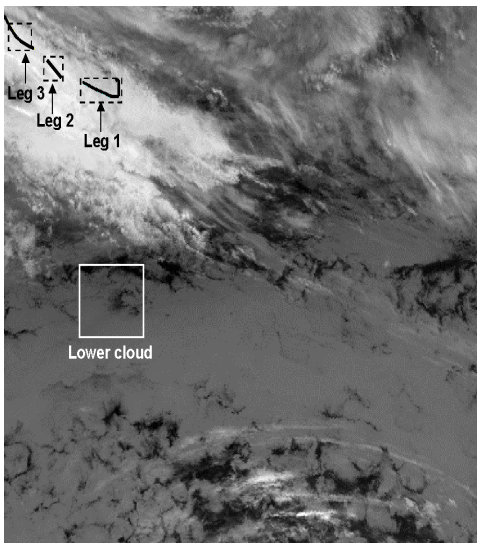

Figure 1: ATSR-2 10.8 µm channel image of the selected region, Pacific Ocean near Punta Arenas, Chile, 23 March 2000.

To correct for the effects of parallax and cloud drift nadir and forward images have to be re-registered with regard to cloud top (Knap et al., 1999). However, automatic methods based on cross correlation between the two images present some problems for thin cirrus overlying lower clouds (Baran et al., 1999a). Consequently, in our case this

process was done by shifting the images by visual inspection.

The region used for our study is shown in Figure 1 for the 10.8 µm nadir channel. This image was acquired by the ATSR-2 instrument around 30 minutes before the in-situ measurements. It shows a large area covered by a broken layer of low level clouds, which in some parts, like in our study area, is overlaid by an optically thin cirrus layer. The dashed line boxes in Figure 1 surrounding the flight legs correspond to those regions used in the following to retrieve the cirrus parameters from the satellite data.

3. MODEL DESCRIPTION

3.1 *Single Scattering by Ice Crystals*

Cirrus clouds are composed of mostly nonspherical ice particles with various shapes and sizes as has been demonstrated by several in-situ observations (Heymsfield and Platt, 1984; McFarquhar et al., 1999). In order to check the most recent theoretical models on light scattering by nonspherical ice crystals we compared theoretical computations with the airborne in-situ measurements of the polar nephelometer. This instrument measures the scattering phase function for scattering angles between 3.5° and 169° of an ensemble of cloud particles that intersect a collimated laser beam at a wavelength of 0.8 µm (Gayet et al., 1997).

Figure 2 (top) shows a comparison of the observed volumetric scattering phase function with the parameterization of Key et al. (2002) for six different ice crystal habits. This parameterization describes the shortwave optical properties of ice clouds for a variety of ice particle habits and mean effective particle sizes and uses a double Henyey-Greenstein function to approximate the phase function. The crosses in Figure 2 represent the polar nephelometer measurements averaged over leg 1 of the flight track (Fig. 1). The calculations are done for the observed mean effective ice particle size and the ice water content averaged over leg 1 and given in Table 1. The most noticeable features of both measured and calculated volumetric scattering cross sections are their smooth shapes and the absence of the 22° and 46° halos. The selected parameterization according to Key et al. (2002) represents the forward scattering reasonably well but it underestimates the backscattering behaviour for every habit. At present, the reason for this behaviour is not known to us. However, any uncertainties in this angular range will affect the retrieval results because the typical scatttering angles for ATSR-2 observations at the considered latitudes of our observations occur in this range.

For comparison, we also calculated the theoretical volumetric scattering cross sections for smooth and rough hexagonal columns using the ice particle size distributions measured by the FSSP-300 and 2D-C probes. The scattering properties for particles with size parameters smaller than 30 were calculated with a new method derived from a generalization of the separation of variables method for infinitely extended hexagonal cylinders (Rother, 1998; Rother et al., 2001). On the basis of this rigorous approach an approximation to finite hexagonal cylinders is obtained by applying the Huygens principle (Rother et al., 1999). For large particles with smooth surfaces we applied the geometric optics approximation and used a ray-tracing program to calculate the single scattering properties of randomly oriented hexagonal ice crystals (Hess and Wiegner, 1994; Wendling et al., 1979). For large particles with rough surfaces the scattering properties were also calculated using a ray tracing method (Macke, 1993; Macke et al., 1996). Forty three different crystal sizes from 3.4 to 700 µm were used to compute the single scattering properties coinciding with the size bins observed by the PMS instruments. For the aspect ratio of hexagonal columns we used empirical relationships between length and diameter reported by Mitchell and Arnott (1994).

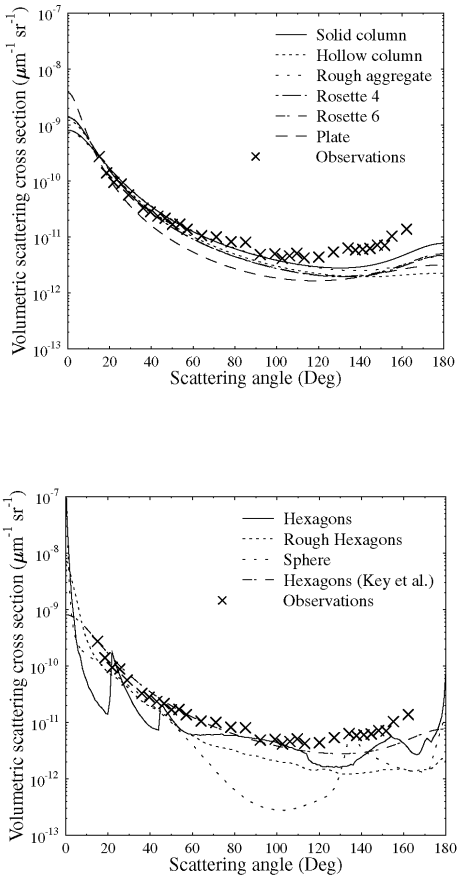

Figure 2: Comparison between volumetric scattering cross sections measured by the polar nephelometer for flight leg 1 and the parameterization by Key et al. (2002) for six different ice particle habits (top), and theoretical results for hexagonal ice columns with smooth and rough surfaces as well as for spheres (bottom).

The volumetric scattering cross sections calculated for leg 1 are shown in Figure 2 (bottom) together with the parameterization for solid hexagonal columns according to Key et al. (2002) and the computation for spherical particles using Mie theory. Again, the theoretical calculations underestimate the observed backscattering. The

most striking feature is the large difference between the scattering functions of spherical and nonspherical particles which exceeds one order of magnitude in the sideward direction. In contrast, all calculations for non-spherical particles are in close enough agreement with the observations to justify the further use of the parameterization by Key et al. (2002) as being representative for the scattering properties of non-spherical ice particles.

3.2 *Radiative Transfer Computations*

For the computation of the radiances observed by the ATSR-2 instrument we used the one-dimensional plane-parallel discrete ordinate method DISORT 2.0 (Stamnes et al., 1988) as part of the libRadtran model package (Kylling and Mayer, 2002). The single scattering properties of ice crystals were calculated using the Key et al. (2002) parameterization described in the previous section. For water clouds we used Mie theory where the droplet size distribution was described by a gamma function. Rayleigh scattering was calculated according to Nicolet (1994) and molecular absorption was parameterized using the three-term exponential sum fitting technique provided by the SBDART radiative transfer mode (Richiazzi et al., 1998) which was for this purpose interfaced to libRadtran. Spectral radiances were calculated over an ocean, weighted with the ATSR-2 spectral responses, and integrated over wavelength. For the thermal channels including the 3.7 µm channel the calculated radiances were converted to brightness temperatures by inversion of the Planck function using the effective wavenumber according to Sospedra et al. (1998).

4. RETRIEVAL METHOD

The retrieval of cirrus cloud parameters such as optical thickness and mean effective particle size from satellite measurements requires the inversion of the radiative transfer model by using the multispectral information contained in spectral bands that are absorbing or nonabsorbing for cloud particles. As Twomey and Cocks (1982) showed for the first time reflectance of clouds depends primarily on cloud optical thickness in nonabsorbing bands (0.87 µm ATSR-2 band) while reflectance at near infrared absorbing wavelengths (1.6 µm and 3.7 µm ATSR-2 bands) depends on both optical thickness and cloud particle size. Making use in addition of the two viewing angles of ATSR-2 we could demonstrate that the retrieval of ice cloud optical thickness and effective particle size is possible even in the presence of a low optically thick water cloud

For this purpose, the retrieval uses first the 0.87, 1.6 and 10.8 µm channel radiances in nadir view to determine in a cirrus cloud free box (Figure 1) the lower cloud optical thickness, effective particle size, and cloud top temperature. In order to reduce the number of parameters we further assume a linear relationship between the optical thickness of the lower cloud and its effective particle size which is confirmed by the analysis of the retrieved parameters for the box depicted in Figure 1 as ‘lower cloud‘ (Fig. 3).

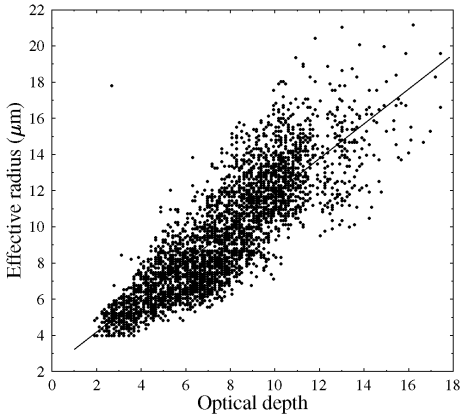

Figure 3: Mean effective particle size of the lower cloud as function of lower cloud optical thickness determined from ATRS-2 data for the box depicted in Figure 1.

The obtained linear relationship is in agreement with previous results on marine stratocumulus (Szczodrak et al. 2001). We assume further that this relationship is also valid in the region below the cirrus cloud and that the lower cloud top temperature determined in the cirrus free region is also valid there.

In a second step, we determine the desired five cloud parameters (cirrus: cloud temperature, optical thickness, effective particle size, predominant particle habit; low level cloud: optical thickness) by using the following five ATSR-2 radiances: the 0.87 µm and 1.6 µm nadir and forward observations, and the 3.7 µm nadir observation. Since the radiative transfer equations cannot be inverted analytically a least square fitting technique was applied by defining a cost function that accounts for the difference between calculated and measured reflectances and brightness temperatures (Nakajima and King 1990). As a consequence of the large range of possible values for every parameter and their independence the defined cost function has several local minima. To find the minima that lead to the lowest values of the cost function we applied the scatter search method (Glover et al. 2001).

5. RESULTS

The new retrieval scheme presented in section 4 was applied to the three boxes containing the flight legs of the aircraft (Fig. 1). Figure 4 shows an example of the relationship between the 0.87 and 1.6 µm reflectances for six different assumed particle habits (Fig. 2) and four different effective particle sizes. The ATSR-2 observations for the box containing flight leg 1 of the aircraft are superimposed as dots.

The results for all three boxes including the flight legs are presented in Table 2.

Table 1. Mean concentration, ice water content, effective crystal size, extinction coefficient, asymmetry parameter, and associated standard deviations (in parenthesis) determined from the in-situ measurements for the three flight legs (Fig. 1).

	Conc. (cm^{-3})	IWC (g/m^3)	$D_{eff,i}$ (μm)	Ext. (km^{-1})	Asym. par.
Leg 1	0.8 (0.7)	0.005 (0.003)	55 (35)	0.25 (0.12)	0.771 (0.006)
Leg 2	2.1 (1.5)	0.011 (0.007)	34 (12)	0.50 (0.30)	0.786 (0.004)
Leg 3	3.9 (2.9)	0.020 (0.010)	47 (20)	1.10 (0.70)	0.773 (0.005)

Table 2. Retrieved mean effective cirrus particle size, optical thickness, temperature, low cloud optical thickness and associated standard deviations (in parenthesis) for the three boxes containing the flight legs (Fig. 1).

	Cirrus cloud			Low cloud
	$D_{eff,i}$ (μm)	Optical depth	Temperature (K)	Optical depth
Leg 1	54.7 (19.9)	0.5 (0.3)	230.1 (9.5)	10.1 (2.1)
Leg 2	51.4 (10.1)	1.2 (0.4)	220.4 (8.5)	4.2 (1.6)
Leg 3	56.4 (14.9)	0.7 (0.2)	227.9 (8.4)	8.1 (1.2)

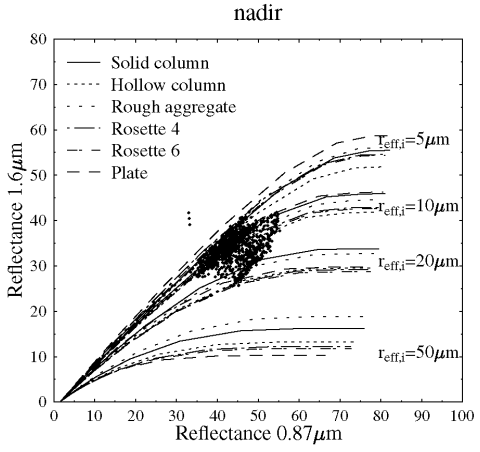

Figure 4: An example of correlations between 0.87 and 1.6μm reflectances. The lines correspond to a variation of optical thickness for different ice particle effective radii and habits. Cirrus temperature is T_i=235.0K, while sun-satellite geometry is (θ_0=65.4º, θ=14.5º and $\Delta\phi$=132.0º) and (θ_0=65.6º, θ=53.7º and $\Delta\phi$=165.0º) for nadir and forward views respectively. Overlapped with the curves are the reflectances for the box containing flight leg 1 (Fig. 1).

The retrieved cirrus cloud optical thickness is very small compared to that one of the lower water cloud, and yet both are clearly separated by the retrieval. Based on the reports of the pilots on the geometrical cloud thickness of 2.2 km and the in-situ measured extinction coefficient of 0.25 km^{-1} the in-situ observations yield an optical thickness for the cirrus cloud of 0.55, which agrees well with the satellite observation.

The best agreement between in-situ measured and retrieved effective ice particle size is obtained for leg 1. This is due to the fact that for optically thin high level clouds the satellite retrieval yields the vertically averaged mean effective particle size. The track of flight leg 1 corresponds to an ascent of the Falcon within the cloud enabling us to calculate the average value from the aircraft data. Measurements for the other legs were carried out at constant altitude. Hence, they are not representative for the whole cloud and especially for leg 2 large deviations between measured and retrieved mean particle sizes occur. The most prominent particle habits obtained from the retrieval of the ATSR-2 data seem to be solid columns, hollow columns and rosettes.

The pixel-to-pixel variability of the lower cloud must be taken into account in order to obtain the properties of the high cloud with reasonable accuracy. Assuming a constant optical thickness of the lower cloud yields for leg 1 an optical thickness of the cirrus cloud which is about three times larger (1.6) than oberved, while the retrieved effectice ice particle diameter is about 7 μm smaller than the observed one. Much larger errors occur when the lower cloud is fully neglected. Our results clearly indicate the need to consider the variability of the optical properties of lower clouds for the retrieval of upper layer cloud properties from satellite data.

Acknowledgement. The authors would like to thank to Hermann Mannstein for processing the ATSR-2 data. This project was partly funded by the European Union within the 5th framework program (EVK2-CT-1999-00039). Additional support was provided by the university of La Laguna enabling Albano Gonzales to carry out this research at DLR.

6. REFERENCES

Baran, A.J., S.J. Brown, J.S. Foot, and D.L. Mitchell ,1999a: Retrieval of tropical cirrus thermal optical depth, crystal size and shape using a dual-view instrument at 3.7 and 10.8μm, *J. Atmos. Sci*., **56**, 92-110.

Baumgardner, D., J.E. Dye, R.G. Knollenberg, and B.W. Gandrud, 1992: Interpretation of measurements made by the FSSP-300X during the Airborne Artic Stratospheric Expedition, *J. Geophys. Res.,* **97***,* 8035-8046.

Gayet, J.F.,, G. Febvre, G. Brogniez, H. Chepfer, W. Renger, and P. Wendling, 1996: Microphysical and optical properties of cirrus and contrails: Cloud field study on 13 October 1989. *J. Atmos. Sci*., **53**, 126-138.

Gayet, J.F., O. Crépel, J.F. Fournol, and S. Oshchepkov, 1997: A new airborne polar Nephelometer for the measurements of the optical and microphysical cloud properties. Part I: Theoretical design. *Ann. Geophysicae*, **15**, 451-459.

Glover, F., M . Laguna and R. Martí, 2001: *Theory and Applications of Evolutionary Computation: Recent Trends,* A. Ghosh and S. Tsutsui (Eds.), Springer-Verlag, in press.

Hess, M., and M. Wiegner, 1994: COP: a data library of optical properties of hexagonal ice crystals, *Appl. Opt.*, **33**, 7740-7746.

Heymsfield, A.J., and C.M.R. Platt, 1984: A parameterization of the particle size spectrum of ice clouds in terms of the ambient temperature and ice water content, *J. Atmos. Sci*., **41**, 846-856.

Key, J., P. Yang, B. Baum, and S. Nasiri, 2002: Parameterization of shortwave ice cloud optical properties for various particle habits, *J. Geophys. Res*., accepted.

Knap, W.H., M. Hess, P. Stammes, and R.B.A. Koelemeijer, 1999: Cirrus optical thickness and crystal size retrieval from ATSR-2 data using phase functions of imperfect hexagonal ice crystals, *J. Geophys. Res*., **104**, 31721-31730.

Knollenberg, R.G., 1981: Techniques for probing cloud microstructure. In *Clouds, Their formation, Optical properties and Effects*, edited by P.V. Hobbs and A. Deepak, pp. 15-92, Academic Press, N.Y.

Kylling, A. and B. Mayer, libRadtran, 1993-2002: A package for radiative transfer calculations in the ultraviolet, visible, and infrared, http://www.libradtran.org.

Macke, A., 1993: Scattering of light by polyhedral ice crystals, *Appl. Opt.*, **32**, 2780-2788.

Macke, A., J. Mueller, and E. Raschke, 1996: Single scattering properties of atmospheric ice crystals, *J. Atmos. Sci*., **53**, 2813-2825.

Mace, G.G., T.P. Ackerman, and E.E. Clothiaux, 1997: A study of composite cirrus morphology using data from a 94-GHz radar and correlation with temperature and large-scale vertical motion. *J. Geophys. Res.*, **102**, 13581-13593.

McFarquhar, G. M., A.J. Heymsfield, A. Macke, J. Iaquinta, and S.M. Aulenbach, 1999: Use of observed ice crystal sizes and shapes to calculate mean-scattering properties and multispectral radiances: CEPEX April 4, 1993, case study, *J. Geophys. Res.*, **104**, 31763-31779.

Mitchell, D.L., and W.P. Arnott, 1994: A model predicting the evolution of ice particles size spectra and radiative properties of cirrus clouds. Part II: Dependence of absorption and extinction on ice crystal morphology. *J. Atmos. Sci*., **51**, 817-832, 1994.

Nakajima, T., and M.D. King, 1990: Determination of the optical thickness and effective particle radius of clouds from reflected solar radiation measurements, I, Theory. *J. Atmos. Sci*., **47**, 1878-1893.

Nicolet, M., 1984: On the molecular scattering in the terrestrial atmosphere: an empirical formula for its calculation in the homosphere, *Planet. Space*. *Sci*., **32**, 1467-1468.

Ou, S.C., K.N. Liou, W.M. Gooch, and Y. Takano, 1993: Remote sensing of cirrus cloud parameters using advanced very-high-resolution radiometer 3.7- and 10.9-μm channels, *Appl. Opt.*, **32**, 2171-2180.

Ou, S.C., K.N. Liou, M.D. King, and S.C. Tsay, 1999: Remote sensing of cirrus cloud parameters based on a 0.63-3.7μm radiance correlation technique applied to AVHRR data, *Geophys. Res. Lett.*, **26**, 2439-2440.

Prata, A.J.F., R.P. Cechet, I.J. Barton, and D.T. Llewellyn-Jones, 1990: The Along-Track Scanning Radiometer (ATSR) for ERS-1: Scan geometry and data simulation, *IEEE Trans. Geosci & Rem, Sens.*, **28**, 3-13.

Ricchiazzi, P., S. Yang, C. Gautier, and D. Sowie, 1998: SBDART: A Research and Teaching Software Tool for Plane-Parallel Radiative Transfer in the Earth's Atmosphere, *Bull. Amer. Meteorol. Soc.,* **79**, 2101-2114.

Rolland, P, K.N., Liou, M.D. King, S.C. Tsay, and G.M. McFarquhar, 2000: Remote sensing of optical and microphysical properties of cirrus clouds using Moderate-Resolution Imaging Spectroradiometer channels: Methodology and sensitivity to physical assumptions, *J. Geophys. Res.*, **105**, 11721-11738.

Rother, T., 1998: Generalization of the separation of variables method for nonspherical scattering on dielectric objects, *J. Quant. Spectrosc. Radiat. Transfer*, **60**, 335-353.

Rother, T., S. Havemann, and K.Schmidt, 1999: Scattering of plane waves on finite cylinders with noncircular cross sections. In *Progress in Electromagnetics Research (PIER)*, **23**, 79-105.

Rother, T., K. Schmidt, and S. Havemann, 2001: Light scattering on hexagonal ice columns, *J. Opt. Soc. Am*., 18, 2512-2517.

Sospedra, F, V. Caselles, and E. Valor, 1998: Effective wavenumber for thermal infrared bands – application to Landsat-TM. *Int. J. Remote Sensing*, **19**, 2105-2117.

Stamnes, K., D. Tsay, W. Wiscombe, and K. Jayaweera, 1988: Numerically stable algorithm for discrete-ordinate-method radiative transfer in multiple scattering and emitting layered media. *Appl. Opt.*, **27**, 2502-2509.

Szczodrack, M, P.H. Austin, and P.B. Krummel, 2001: Variability of optical depth and effective radius in marine stratocumulus clouds, *J. Atmos. Sci.*, **58**, 2912-2926.

Twomey, S. and T. Cocks, 1989: Remote sensing of cloud parameters from spectral reflectance in the near-infrared. *Beitr. Phys. Atmos*., **62**, 172-179.

Wendling, P., R. Wendling, and H.K. Weickmann, 1979: Scattering of solar radiation by hexagonal ice crystals, *Appl. Opt.*, **18**, 2663-2671.